

RSC Advances



This is an *Accepted Manuscript*, which has been through the Royal Society of Chemistry peer review process and has been accepted for publication.

Accepted Manuscripts are published online shortly after acceptance, before technical editing, formatting and proof reading. Using this free service, authors can make their results available to the community, in citable form, before we publish the edited article. This *Accepted Manuscript* will be replaced by the edited, formatted and paginated article as soon as this is available.

You can find more information about *Accepted Manuscripts* in the [Information for Authors](#).

Please note that technical editing may introduce minor changes to the text and/or graphics, which may alter content. The journal's standard [Terms & Conditions](#) and the [Ethical guidelines](#) still apply. In no event shall the Royal Society of Chemistry be held responsible for any errors or omissions in this *Accepted Manuscript* or any consequences arising from the use of any information it contains.

Formation of Lepidococite (γ -FeOOH) from Oxidation of Nanoscale Zero-Valent Iron (nZVI) in the Oxygenated Water

Airong Liu^{a,b}, Jing Liu^{a,b}, Bingcai Pan^{a,c}, Wei-xian Zhang^{a,b*}

^a*State Key Laboratory for Pollution Control and Resource Reuse*

^b*College of Environmental Science and Engineering,*

Tongji University, Shanghai, China, 200092

^c*School of the Environment, Nanjing University, Nanjing, China, 210093*

Abstract

To assess the aquatic reactivity, toxicity, fate and transport of nanomaterials, it is essential to determine their transformation in composition, morphology and surface characteristics in water. In this work, oxidation products of nanoscale zero-valent iron (nZVI) are characterized with spherical aberration corrected scanning transmission electron microscopy (Cs-STEM) integrated with selected area electron diffraction (SAED) and energy-dispersive X-ray spectroscopy (EDS). Crystalline structures from nZVI oxidation in oxygenated water were identified. Methods of Cs-STEM, EDS, X-ray diffraction (XRD), Raman spectroscopy, and X-ray photoelectron spectroscopy (XPS) all prove that the main product is oxyhydroxides (FeOOH), notably lepidococite (γ -FeOOH).

* To whom correspondence should be addressed. Tel: +86-21-6598-2684; Fax: +86-21-6598-3689

E-mail address: zhangwx@tongji.edu.cn (Wei-xian Zhang)

Nanoscale zero-valent iron (nZVI) is one of the most widely applied nanomaterials applied in groundwater remediation and hazardous waste treatment.^{1,2} With the number of field applications growing rapidly, aspects related to its environmental stability, mobility, long-term fate and toxicological impact have received increasing attentions.³⁻⁵ Particularly, concerns over the potential negative impact of nZVI applications have spurred a number of studies examining the chemical and biological characteristics of nZVI.⁶⁻⁹ For example, research showed that bacterial exposure to nZVI can cause disruptions to the cell membranes and leakage of intracellular contents.⁶ Studies on the effects of nZVI on Medaka fish indicated that oxidative damage can be induced in the embryos.⁷ Research further suggested that the toxic effect is significantly lower when nZVI is oxidized⁶ or in the presence of an environmental matrix, such as natural organic matter (NOM).⁸

nZVI has a textbook core-shell structure, which is formed spontaneously in water.¹ The Fe(0) core can be oxidized to form iron [Fe(II) and Fe(III)] oxides upon reactions with water, dissolved oxygen and other oxidants including a large number of environmental contaminants.¹⁰⁻¹⁵ Furthermore, iron oxides can exist in a bewildering variety of polymorphs, as many as 16 distinct species in the form of oxides, hydroxides, and oxyhydroxides have been identified.^{16,17} Most forms of iron oxides are widely distributed in the natural environment and can participate in a variety of biogeochemical processes in the lithosphere, atmosphere, hydrosphere and biosphere. Researches on the ZVI oxidation or aging have so far identified several products, including goethite (α -FeOOH), akaganeite (β -FeOOH), lepidocrocite (γ -FeOOH), magnetite (Fe_3O_4), maghemite (γ - Fe_2O_3), green rusts I/II (a group of bluish-green Fe(II)-Fe(III)

hydroxyl salts), siderite (FeCO_3), and iron sulfide, etc.¹⁰⁻¹⁵

Objective of this work is to conduct atomic scale characterizations on the transformation of nZVI in oxygenated water, especially on the nanostructures of fully oxidized nZVI. To understand surface chemistry of nZVI, assess its activity, aggregation, fate and transport, eco- and human toxicity, it is essential to determine precisely the eventual product(s), that is, the exact type or form of iron oxides. In this work, a state-of-the-art spherical aberration corrected scanning transmission electron microscopy (Cs-STEM) was applied to generate near atomic resolution physical imaging and chemical identification of nZVI. The spherical aberration corrector allows a larger probe current to be focused in a very fine probe, making atomic resolution spectroscopy possible.¹⁸⁻²²

To examine the transformation of nZVI in water, images of the fresh nZVI particles are needed (Fig.1). Nanoparticles synthesized from the borohydride reduction of ferric ions have a core-shell structure with a metallic core surrounded by a thin shell. As shown in the figure, the particle diameter was ~ 60 nm while the shell thickness was about 3-5 nm.^{21,23} Average BET surface area was in the range of 25-35 $\text{m}^2\cdot\text{g}^{-1}$. Total iron content was approximately 90.3%. Metallic iron [Fe(0)] content was measured at 75.9%.²³ The nanoparticles can form chain-like clusters because of the magnetic forces and electrostatic interactions.

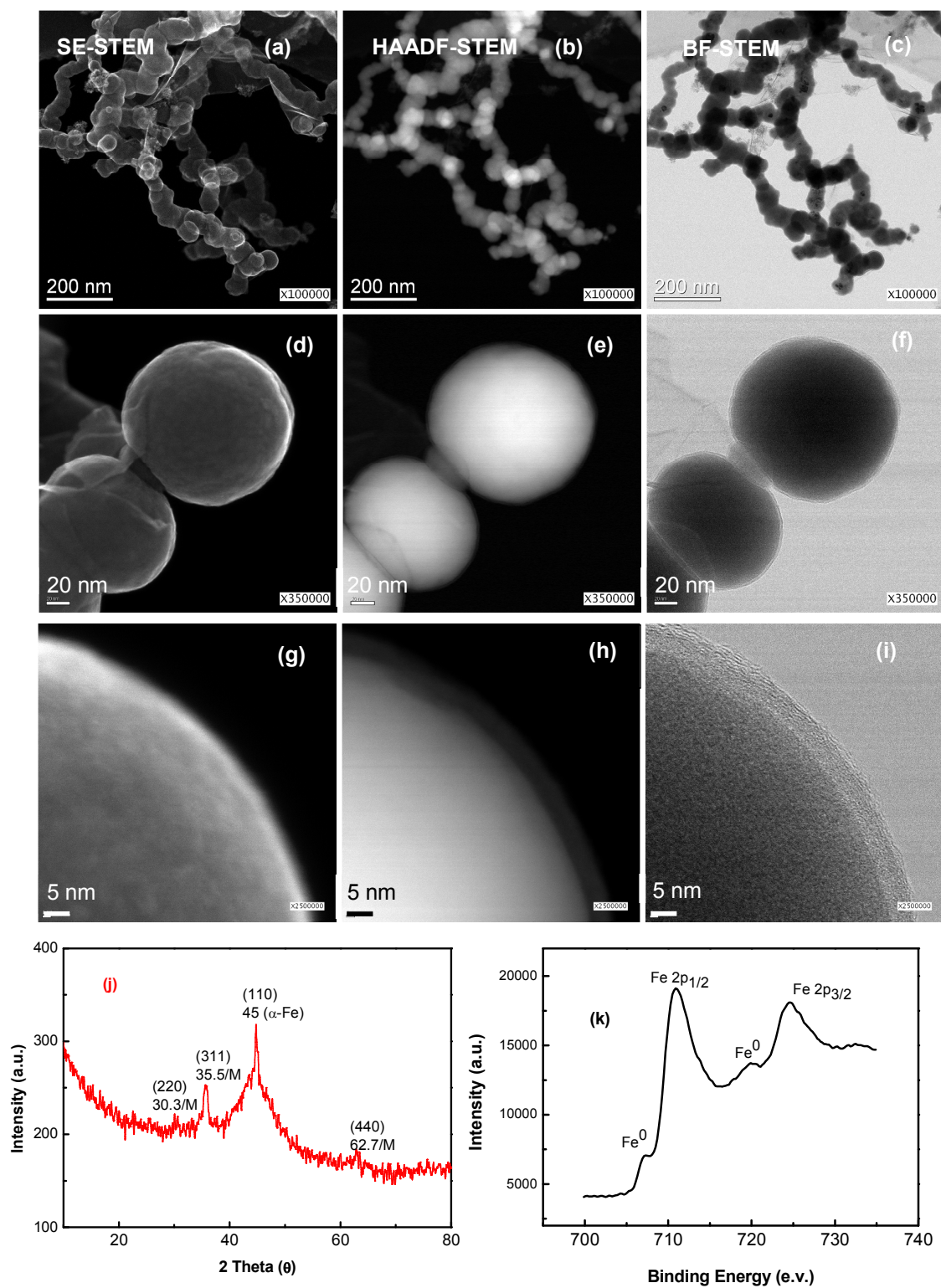


Fig. 1 STEM images of fresh nZVI acquired with a Hitachi HD2700 STEM: (a, d, g) are secondary electron (SE) images, (b, e, h) high-angle annular dark field (HAADF) images, and (c, f, i) bright field (BF) images. (j) is the XRD spectrum, and (k) is the XPS response of Fe 2p core levels of fresh nZVI.

The SE images (Figs.1 a, d, g) offer near three-dimensional, spherical perspectives of the nZVI particles. Images constructed from the secondary electron diffraction clearly present rich depth information about the particle surface. Figs.1b, e, h show a series of STEM-HAADF images of nZVI. HAADF images are often described as the Z-contrast (atomic number) imaging since the measured intensity is approximately proportional to the square of the atomic number, is a high-resolution technique that generates readily interpretable images of nanoscale structures,¹⁸⁻²² that is, regions of the specimen with greater atomic number appear brighter in the image. For example, the particles in Figs 1b, e, h consist of a bright core, corresponding to the metallic iron while the outer layer containing oxygen and iron is darker than the core area.

In the XRD spectrum of fresh nZVI (Fig 1j), peaks at the 2θ of about 45° and $35.5, 63^\circ$ signal the presence of both iron [α -Fe(0)] and iron oxide crystalline phases. The broad peak at about 45° suggests the existence of small grains in the metallic core of nanoparticles.²¹

The two nano components of fresh nZVI are further confirmed by the XPS characterization shown in Fig. 1k. The photoelectron peaks at ~ 711 eV, ~ 720 eV and ~ 724 eV represent the binding energies of Fe $2p_{3/2}$, shake-up satellite $2p_{3/2}$ and $2p_{1/2}$, respectively.²⁴ Those feature peaks confirm that the surface of iron nanoparticles is mainly composed of a layer of iron oxides while the smaller peak at 706.5 eV is assigned to zero-valent iron ($2p_{3/2}$).

Figure 2 presents SE, HAADF and BF images of the oxidized nZVI. After reactions with oxygen and water for 72 hours under completely mixed conditions, the core-shell structure totally collapsed. The nZVI particles underwent complete transformation from metal iron (Fe^0) to iron oxide/hydroxides, resulting complete variations in structure and composition.¹⁰⁻¹⁴ Products from the nZVI oxidation are mostly thin layers of sheets or bundles of needles-shaped crystals, characteristic of iron oxides. As a result of the iron oxidation, Fe(II) diffuses outward from the core area and forms an oxide phase on the surface. Given sufficiently time and oxygen, complete loss of the Fe(0) core and emergence of hollowed-out oxide shells was observed.¹ Previous research on the nZVI oxidation under flowing conditions also indicated that a multiphase oxidation process may be possible including iron oxidation, dissolution, ion migration among particles, and migration and reagglomeration of unoxidized or partially oxidized particles.²⁴ Additional STEM images on the oxidized nZVI can be found in the Supporting Information (Fig. S1). The little dotlike structures in the Figure S1 (a-c) illustrate the possible dissolution–reprecipitation mechanism responsible for the products formation.

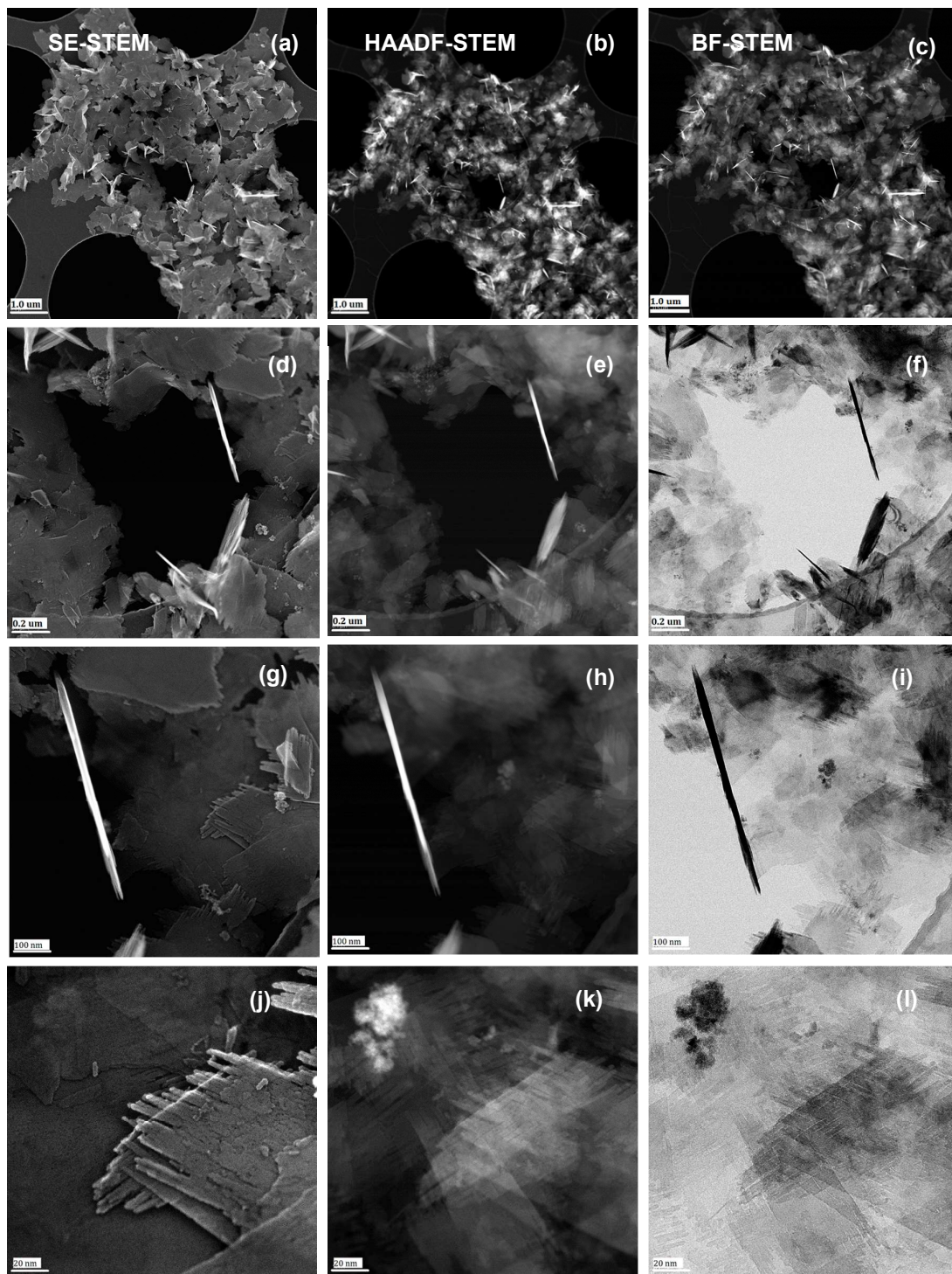


Fig. 2 STEM images of oxidized nZVI: SE (a, d, g, j), HAADF (b, e, h, k) and BF (c, f, i, l) images after 72 h in oxygenated water.

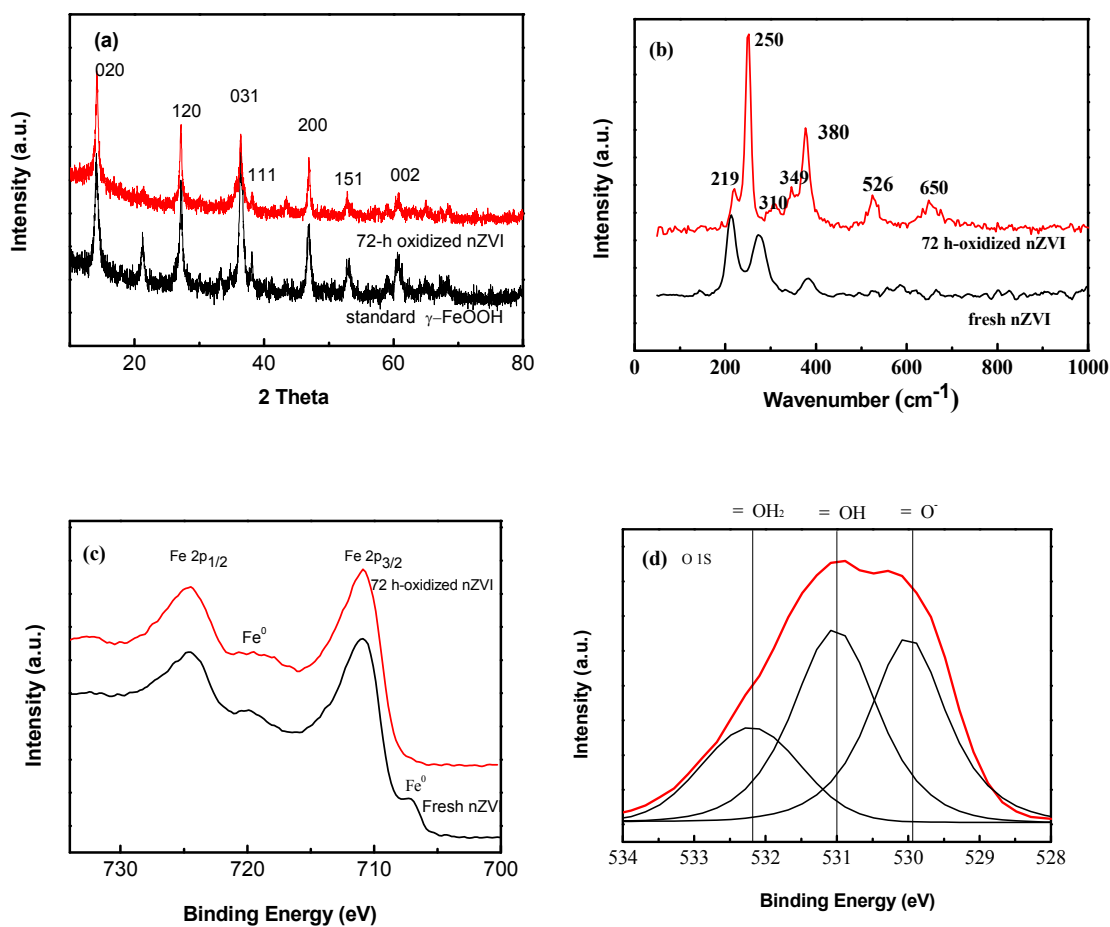


Fig. 3 XRD, XPS and Raman spectroscopy of oxidized nZVI: (a) XRD pattern of the fresh and oxidized nZVI, and standard sample of γ -FeOOH from Aldrich, (b) Raman spectroscopy of the fresh and 72-h oxidized nZVI, (c) XPS of Fe 2p of the fresh- and oxidized nZVI, and (d) O 1s of oxidized nZVI.

The oxidized nZVI nanoparticles are further analyzed with three independent techniques to determine its structural and compositional changes. Figure 3 (a) shows four typical peaks of lepidocrocite at: 14.2 (020), 27.1(120), 36.5(031), 47.0 (220) (PDF#01-0136) in the X-ray diffractiongram of the oxidized nZVI ²⁶. At the same time, the XRD patterns of the 72-h oxidized nZVI are almostly similar to that of the standard γ -FeOOH sample from Aldrich. Thus, γ -FeOOH is likely the main mineral for nZVI aged in water. In a previous study on the aqueous-phase carbon-steel corrosion, goethite (α -FeOOH) was identified as the predominant product under simulated feedwater conditions.²⁶

In this study, products of the nZVI aged in water for 2 h, 12 h, 48 h, 72 h were analyzed with XRD (Fig. S2). The XRD patterns of 72h nZVI are similar to that of 48-h- oxidized nZVI, suggesting that nZVI is fully oxidized after 48 hours in water. The typical XRD peaks for iron oxides, (oxy) hydroxides mineral phase of nZVI aging products are listed in Table 1.

Table 1 XRD peaks for iron oxides, (oxy) hydroxides mineral phase of nZVI aging products

Iron Oxides (oxy)hydroxides	2 θ (°)	Reference
γ -Fe ₂ O ₃ / Fe ₃ O ₄	30.3 (220), 35.6 (311), 43.5 (400), 57.2 (511), 62.7 (440)	(10,11)
γ -FeO(OH)	14.2(020), 27.1(120), 36.5 (031), 47.0 (020) , 38.1(111), 43.5(131), 52.9(151), 58.8(080), 60.9 (231), 68.4 (251)	(26)

Bold numbers represent very strong, typical for the γ -FeO(OH) ^[26].

The presence of γ -FeOOH as an oxidization product is favored by the continuous stirring, which supplies the solution with sufficient oxygen to maintain fully oxygenated conditions. The results observed on the oxide formation suggest that corrosions of nZVI favor formation iron oxyhydroxide (FeOOH) over iron oxides, which can be described by the following reactions:

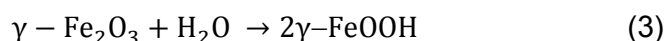
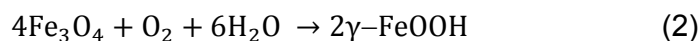
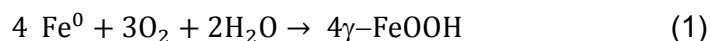


Fig. 3b presents Raman spectra of fresh- and 72-h oxidized nZVI. The spectrum of γ -FeOOH has characteristic peaks at 219, 250, 311, 349, 379, 528, and 648 cm^{-1} .²⁷ The high intensity peaks are 250 and 379 wavenumbers for the 72-h-oxidized nZVI, which are in good agreement with the Raman spectroscopy characteristics of γ -FeOOH reported in the literature.²⁷

A detailed characterization of fresh- and 72-h-oxidized nZVI was also performed with XPS. Fig. 3c shows the survey of Fe 2p core levels, peaks at 710.56 eV, 719.26 eV and 723.91 eV represent the binding energies of Fe ($2p_{3/2}$), shake-up satellite $2p_{3/2}$ and $2p_{1/2}$, respectively.²⁴ The three feature peaks suggest that the 72-h nZVI surface consists of mostly iron oxides and hydroxides. The peak at ~ 711 eV suggests the potential presence of Fe_2O_3 , Fe_3O_4 , $\text{Fe}(\text{OH})_3$, or FeOOH, while the one at ~ 725 eV indicates the presence

of ferric oxides [Fe(III)].²⁴ Since both Fe₂O₃ and FeOOH have similar XPS features and peak positions in this region, O1s survey scans are thus analyzed to delineate the surface oxygen states (Fig. 3d). The O 1s region can be decomposed into three peaks at 529.9, 531.0 and 532.5 eV, corresponding to O²⁻, OH, and chemically or physically adsorbed water, respectively.²⁴ The existence of surface -OH group suggests that the oxidized iron is likely in the state of FeOOH. If the surface structure is Fe₂O₃, a single peak at ~530 eV would have been observed. The ratio of OH to O²⁻ is approximately 1.09, in agreement with the bulk FeOOH stoichiometry and comparable with reported values of 0.9-1.1, 1.03, and 0.9.²⁴ In short, the XPS results fully support that FeOOH is the major component of oxidized nZVI.

To further verify the crystal phase of the surface oxyhydroxides, fine structure of a single nanosized needle was studied with high resolution (HR) STEM (Fig 4). As can be seen from the BF images (Fig. 4a), the needle-like nanostructure is present alone with diameter at ca.10 nm. The high resolution images reveal the crystalline nature with an interplanar spacing of 3.29 and 2.46 Å (Fig. 4c), which match well with the (120) and (031) planes of orthorhombic structured lepidocrocite.²⁶ The selected area electron diffraction (SAED) patterns (Fig. 4b inset) and HR-STEM (Fig. 4c) both indicate that those lepidocrocite nanorods are clearly of single crystal. The EDS spectrum (Fig. 4d) confirms the existence of Fe and O elements in the products, offers complementary evidence on the formation of iron oxyhydroxides. All

information obtained from the independent techniques support that the needle-like product is indeed lepidocrocite.

It should be noted here that the needle-shape morphology is also characteristic of goethite, but our XRD analysis clearly confirms that the crystal phase belongs to lepidocrocite, not goethite. Oxidation of nZVI by water and oxygen produces both ferrous and ferric iron. The behavior of Fe (II) was confirmed in two aspects, catalytic dissolution-reprecipitation and catalytic solid-state transformation.²⁸ The continuous oxygen supply as well as the existing of Fe (II), provide favorable conditions to form (oxy)hydroxides polymorphs.²⁸ The formation of lepidocrocite starts with nZVI dissolution and is followed by the reprecipitation of solid products. On the other hand, the needle-like shape could also be an intermediate morphology. Thus aging of nZVI in oxygenated water yields well-formed lepidocrocite crystals, and may further evolve to more stable sheet-shaped products.

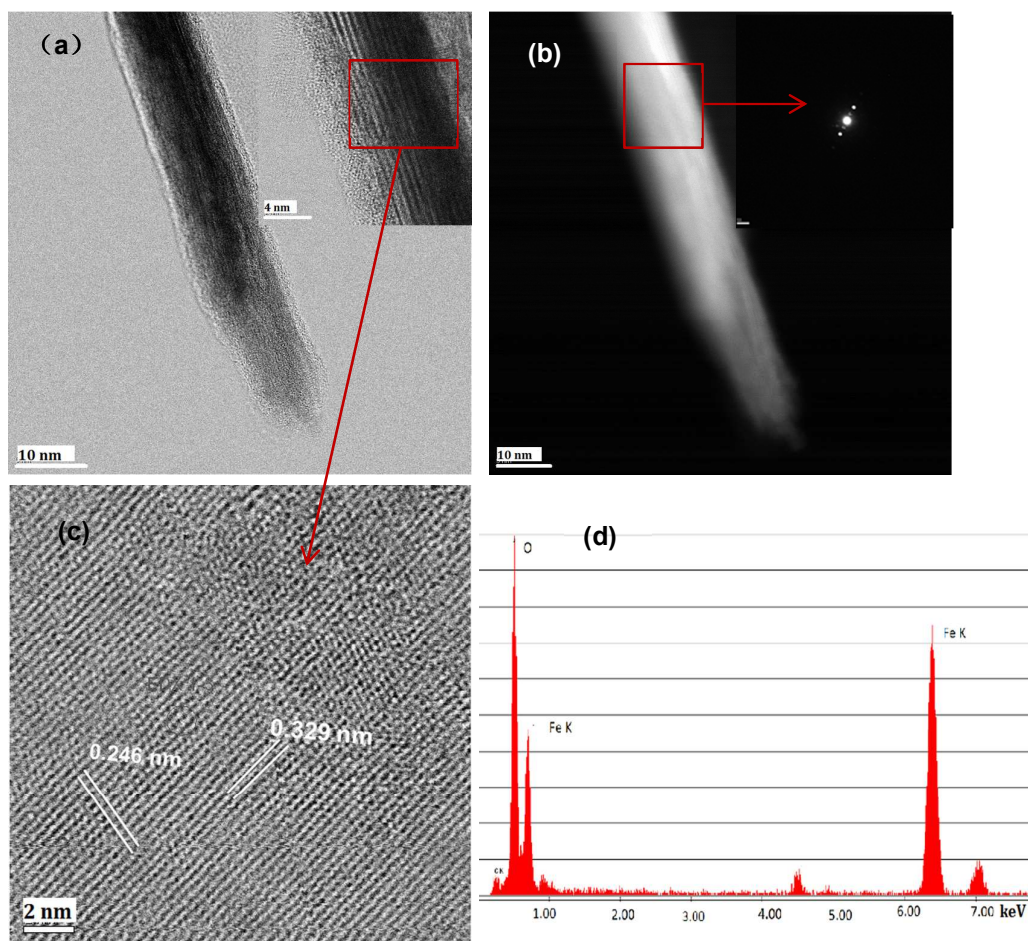


Fig. 4 High resolution images of oxidized nZVI: (a) BF image, (b) DF image, (c) HR-STEM image and (d) EDS spectrum of 72-h oxidized nZVI. Insert of (a) is an enlarged image for the selected area (red box) of the left image. Inset of (b) is the SAED of elected area (red box) of the needle-shaped image.

Conclusions

In this work, the final corrosion products of nZVI in the stirring water are studied using a combination of STEM, SAED, EDX, XRD, XPS, and Raman spectra. Images acquired by a Hitachi HD-2700 STEM provide that after fully oxidized in stirred aquatic water for 72h, the core-shell structured nZVI collapse and generate lath-like and bundles of thin needles-shaped crystals.

XRD, XPS and Raman spectra analysis prove the formation of lepidococite. Patterns of SAED suggest single crystalline structures for the lepidococite. The evidence of γ -FeOOH formation is significant for the understanding on nZVI surface chemistry, and to assess its surface charge, colloidal stability and aggregation in water, also sorption of natural organic substances and heavy metal ions in aquatic systems.

Acknowledgements

This work has been partially supported by the National Science Foundation of China (NSFC Grants 21277102 and 21003151) and the Fundamental Research Funds for the Central Universities (20123211). The authors thank Hitachi High-Technologies Corporation for the use of HD-2700 STEM.

Notes and references

1. W. L. Yan, H.-L. Lien, B. E. Koel and W.-X. Zhang, *Environ. Sci.: Processes Impacts*, 2013, **15**, 63–77.
2. B. J. Kharisov, R. Dias, O. V. Kharissova, V. M. Jiménez-Pérez and F. B. Muñoz, *RSC Adv.*, 2012, **2**, 9325-9358.
3. D. W. Elliott and W.-X. Zhang, *Environ. Sci. Technol.*, 2001, **35**, 4922-4926.
4. B. C. Reinsch, B. Forsberg, R. L. Penn, C. S. Kim and G. V. Lowry, *Environ. Sci. Technol.*, 2010, **44**, 3455–3461.
5. R. L. Johnson, J. T. Nurmi, G. S. O. Johnson, D. Fan, R. L. O. Johnson, Z. Shi, A. J. Salter-Blanc, P. G. Tratnyek and G. V. Lowry, *Environ. Sci.*

- Technol.*, 2013, **47**, 1573–1580.
6. C. Lee, J. Y. Kim, W. I. Lee, K. L. Nelson, J. Yoon, and D. L. Sedlak, *Environ. Sci. Technol.*, 2008, **42**, 4927-4933.
7. H. Li, Q. Zhou, Y. Wu, J. Fu, T. Wang and G. Jiang, *Ecotox. Environ. Safety*, 2009, **72**, 684-692.
8. Z. Li, K. Greden, P. J. J. Alvarez, K. B. Gregory and G. V. Lowry, *Environ. Sci. Technol.*, 2010, **44**, 3462–3467.
9. Q. Chen, J. Li, Y. Wu, F. Shen and M. Yao, *RSC Adv.*, 2013, **3**, 13835-13842.
10. H.-S. Kim, J.-Y. Ahn, K.-Y. Hwang, I.-K. Kim and I. Hwang, *Environ. Sci. Technol.*, 2010, **44**, 1760–1766.
11. Q. L. Wang, S. Snyder, J. Kim and H. Choi, *Environ. Sci. Technol.*, 2009, **43**, 3292–3299.
12. V. Sarathy, P. G. Tratnyek, J. T. Nurmi, D. R. Baer, J. E. Amonette, C. L. Chun, R. L. Penn and E. J. Reardon, *J. Phys. Chem. C*, 2008, **112**, 2286-2293.
13. T. Satapanajaru, P. J. Shea and S. D. Comfort, *Environ. Sci. Technol.*, 2003, **37**, 5219-5227.
14. S. R. Kanel, B. Manning, L. Charlet and H. Choi, *Environ. Sci. Technol.*, 2005, **39**, 1291-1298.
15. J. Klausen, P. J. Vikesland, T. Kohn, D. R. Burris, W. P. Ball, and A. L. Roberts, *Environ. Sci. Technol.*, 2003, **37**, 1208-1218.

16. A. Navrotsky, L. Mazeina and J. Majzlan, *Science*, 2008, **319**, 1635-1638.
17. T. Ahn, J. H. Kim, H.-M. Yang, J. W. Lee and J.-D. Kim, *J. Phys. Chem. C*, 2012, **116**, 6069-6076.
18. S. J. Pennycook and L. A. Boatner, *Nature*, 1988, **336**, 565–567.
19. P. E. Batson, N. Dellby and O. L. Krivanek, *Nature*, 2002, **418**, 617–620.
20. D. A. Muller, N. Nakagawa, A. Ohtomo, J. L. Grazul, and H. Y. Hwang, *Nature*, 2004, **430**, 657–661.
21. A. R. Liu and W.-X. Zhang, *Analyst*, 2014, **139**, 4512-4518.
22. L. Ling and W.-X. Zhang, *RSC Adv.*, 2014, **4**, 33861-33865.
23. J. Cao, X. Li, J. Tavakoli and W.-X. Zhang, *Environ. Sci. Technol.*, 2008, **42**, 3780–3785.
24. X. Q. Li, and W.-X. Zhang, *J. Phys. Chem. C*, 2007, **111**, 6939-6946.
25. L. F. Greenlee, J. D. Torrey, R. L. Amaro and J. M. Shaw, *Environ. Sci. Technol.*, 2012, **46**, 12913–12920.
26. G. B. McGarvey, K. B. Burnett and D. G. Owen, *Ind. Eng. Chem. Res.*, 1998, **37**, 412-419.
27. M. K. Nieuwoud, J. D. Comins and I. Cukrowski, *J. Raman Spectrosc.*, 2011, **42**, 1335-1339.
28. D. D. Boland, R. N. Collins, C. J. Miller, C. J. Glover and T. D. Waite, *Environ. Sci. Technol.*, 2014, **48**, 5477–5485.